This is a Peer Reviewed Paper
FIG Congress 2022

Fusion of inhomogeneous geodetic data for Rock Cliff Monitoring: a Case Study of the Lianziya Cliff in Three Gorges National Geological Park in China

Aiham Hassan, Li Zhang, Gabriel Kerekes, Volker Schwieger, Germany

Key words
Engineering survey, GB-SAR, GNSS, TLS, Monitoring, Inhomogeneous data, Rock fall

SUMMARY
Rock cliff monitoring on the Yangtze riverside is of crucial importance for the inhabitant's life, waterborne transportation and the Three Gorges Dam. The Lianziya Cliff is in a high-risk area and requires geodetic monitoring for collapse predictions. This is achieved with different measurements techniques that co-work with the purpose of determining cliff movements. This publication shows the fusion of tachymeter, GNSS (Global Navigation Satellite System), GB-SAR (Ground based Synthetic Aperture Radar) and TLS (terrestrial laser scanner) data and reaffirms the stability of the cliff within a period of one year. One challenge is to combine data represented in different dimensions, for e.g. GB-SAR data which gives line-of-sight displacements and area-wise TLS point clouds that are directly in 3D, as well as point-wise Total Station (TS) and GNSS. Another challenge was to define a common geodetic reference for the two epochs and to detect movements or deformations between two epochs. In principle, this should not be so difficult, but often, as in this case, the measurements are inhomogeneous or even not complete in each epoch. In this contribution the authors focus on solving these issues e.g. by TS measurements and the Iterative Closest Point (ICP) algorithm. The two epochs took place in 2018 and 2019; time interval that is too small to detect deformations. Therefore, statements regarding the required temporal distance to detect deformations are also made.

Fusion of inhomogeneous geodetic data for Rock Cliff Monitoring: a Case Study of the Lianziya Cliff in Three Gorges National Geological Park in China

Aiham Hassan, Li Zhang, Gabriel Kerekes, Volker Schwieger, Germany

1. INTRODUCTION

Our world is dynamic and changes continuously. Human activities accelerate this natural change increasingly in the last decades. In order to avoid or at least reduce the risks caused by these changes (e.g. landslides, earthquakes) it is important to detect the changes at an early time and thus to apply suitable actions like stabilization or even evacuation. Deformation measurements are widely used for change detection. Nowadays numerous deformation measurement methods are available. The choice of the suitable method depends on the deformations scenario for example properties of the monitored object (dimension, geometry, material and reflectivity), expected deformation magnitude and speed and the risk degree (for contact or contactless measurement). However, each measurement method has limits. For this reason, it is recommended to combine measurement methods in order to get reliable results. However, the data acquired by different measurement methods are generally inhomogeneous, so the data fusion in this case is more challenging.

In this paper, an approach for monitoring of Lianziya rock cliff will be described. Data from several geodetic sensors that imply point-wise and area-wise measurement methods are used in an overarching manner, with the goal of data fusion for monitoring purposes. The results from individual deformation analyses of point-wise (GNSS and tachymeter) and area-wise methods (TLS and GB-SAR) are presented separately and then an attempt for data fusion is made. Throughout the paper, intricacies that occurred during the two measurement campaigns separated by one year and problems with data processing are presented. The encountered problems, solutions to them and unsolvable issues, should help the reader in decision making for similar multi-sensor monitoring systems.

Lianziya is located in China on the southwest bank of the Yangtze River and 27 km upper Three-Gorges Dam. The rock cliff is unstable due to natural conditions (e.g. active geological structure) as well as human activities (e.g. coal mining). According to the geological structure, topography and deformation characteristic Linaziya is divided into three areas (for more details about these areas see Hassan et al. 2018, Wang 1999). Area 1 could be stabilized using constructive measures (Yi 2006). However, an investigation in areas 2 and 3 indicates that area 3 still active with an annual horizontal displacement up to 4.2 mm to the valley (north-east direction) and an annual vertical displacement up to 2.9 mm (Tu and Wu 2011). For this reason just area 3 will be considered in this paper. In figure 2, this area is named by “active area”.

Within the monitoring approach, three monitoring methods are applied. These are GNSS (Global Navigation Satellite System), TLS (terrestrial laser scanner) and GB-SAR (Ground based Synthetic Aperture Radar). Measurements data from each method are gathered at two different epochs: March 2018 and September 2019. The data from those methods and epochs are fused afterwards. For fusion of this inhomogeneous data, it is necessary to transform them into a unique coordinate system. This coordinate system is achieved using GNSS and total

station (TS) in 2019, and only by GNSS in 2018. The deformation analysis is done through two-epoch comparison and under the justified assumption, that the monitoring site is stable during the measurement period of each epoch. Since the measurement epochs are only separated by one year, the movements would have been detected only in case of larger than expected displacements or of more accurate geo-referencing through GNSS and tachymeter. Therefore, the focus is on describing the fusion and identity possible shortcomings of the design as well as possible statements regarding the required temporal distance (monitoring sampling rate) to detect deformations.
In the following, the characteristic of possible monitoring measurement methods generally will be discussed. After that, the test scenario for the case study proposed here including the properties of the monitoring site and the used measurement approach will be presented. Subsequently the data acquisition and processing of each measurement method are described. Afterwards the data fusion approach is highlighted. Finally, the results and statements with respect to deformation analysis are presented and discussed.

2. OVERVIEW AND CHARACTERISTICS OF THE MEASUREMENT METHODS

Monitoring of artificial structures, such as bridges, tunnel, tower, and natural objects such as landslides, glacier, rock cliffs, is one of the main tasks of engineering geodesy. Traditional geodetic instruments are for example GNSS (Global Navigation Satellite System) receiver system, total station. Both of them enable the pointwise measurement of 3-dimensional position directly. For point-wise measurement methods, the measurement points should be signalized, which is laborious and sometimes difficult or impossible in practice. Generally, the geodetic measurement methods can detect deformation on the surface of the monitoring objects, to "look inside" the monitoring object and the find out the internal deformation within the monitoring objects (e.g. landslides) and reasons for the deformation, many geotechnical measurements instruments, such as extensometer, inclinometers, plumbing, alignment are widely used for monitoring application. In the recent years, the fibre optic sensors are integrated in the monitoring object for real time in practice (e.g. Lienhart et al 2019). The geodetic and geotechnical techniques are complementary to each other and used in combination in many monitoring projects (Hesse et al 2016, Ryf et al 2017), therefore close interdisciplinary cooperation of geodesists and geotechnical engineers is essential for monitoring tasks.
Rapid development of performance of computers and communication technologies enables continuous, automatic and cost-effective monitoring. For instance, geosensor networks (GSN) with the low-cost GNSS receiver system for monitoring application are introduced in Heunecke et al. (2011) and Zhang et al. (2012). In recent years the cost-effective mini-computer, such as Raspbeery Pi, were widely used in GSN (Schliefelbein and Stemphuber 2020, Engel et al. 2020). Every sensor node in GSN contains different kinds of data acquisition sensors/instruments and be regarded as multisensory system. Besides, they contain also the modules for data communication and autonomous power supply. The GSNs are installed on the monitoring objects permanently at least during the project duration, so that the continuous data acquisition is realized. Also a total station network including reflectors may be understood as GSN. Furthermore, more and more open source software are available for monitoring application, e.g. there is open source JAG3D (Steinbeis Transfer Centre Applied Geodesy 2020)

for adjustment and OpenADMS for sensor control, observation data processing in GSN (Engel and Foppe 2016). With the development of cost-effective hardware and software, more sensors could be applied or more points could be observed, so that spatial sample of data acquisition could be increased slightly.

While the continuity and automation increase the data acquisition temporally, the data acquisition sample is also increased spatially by measurement methods essentially, such as laser scanning (terrestrial and airborne), photogrammetric (terrestrial and airborne), radar (satellite and ground based synthetic aperture radar), so that the monitoring objects can be observed in area-wise.

In general, in contrast to point-wise measurement methods, area-wise measurement methods have much higher spatial resolution than point-wise measurement methods and are contactless and therefore the signalization of the measurement point is often not required. However, if epoch-wise monitoring tasks (measurement periods are interrupted for defined time intervals) are considered, one may need identical signalized or non-signalized individual points for registration or geo-referencing or, at least, to relate the epoch data among each another (e.g. interepochal registration of TLS data).

However, area-wise measurement methods take at least several seconds to finish the measurement of one area, so that they are generally not suitable for detecting the high dynamic deformation or behaviours of the object up to now. Schill and Eichhorn (2017) show an innovative method for detection of dynamic behaviours (vibration) of bridge with profile laser scanner with a measurement rate of at least of 50 Hz, however only 2D-profile at one position is measured and processed. This is sufficient for the intended application, but not generally applicable for other monitoring applications.

Furthermore, the area-wise measurement methods are general suitable for documentation propose and generation of 3D-model, such as as-built documentation for construction purpose and generation of DTM, because the geometry of the objects could be acquired very detailed. However, area-wise measurement methods meet many challenges for monitoring application. Firstly, the single measurement point is not reproducible, that means the measurement of different epochs cannot be compared directly, which makes the deformation analysis more challenging. Therefore, some deformation analysis methods base on modelling of point cloud data. If the surface structure is quite regular and could be approximated by some geometry primitives such as that of dam or other some artificial structure the modelling could be simple. However, the modelling of the irregular surface, such as that of cliffs and landslides will be more challenging. Harmening and Neuner (2017) used the NUBRBS (Non-Uniform Rational B-splines) for the approximation of the surface, which provides more flexibility for modelling. Moreover, the direct line-of sight must be given for area-wise measurement methods, and the reflection property of the object surface plays a very important role, enough points should be reflected, so that the objects could be reconstructed completely and correctly.

The received signal by the area-wise measurement methods is actually an average value of one area with limited extension on the object surface. The exact form and size (about several mm) of the beam footprint depend on the structure of the object surface and the angle of incidence. Depending on the distance between the radar instrument and monitoring object, the size of footprint of radar could be several meters, so that it will be difficult to get the detailed deformation of small areas.

From the radar interferometer, only the distance change in the line-of-sight could be measured (only one dimension), the deformation in the interested coordinate component could only be derived if the DTM is available. The distance change in line-of-sight can be measured in sub-mm by radar, however, if distances change more than ¼ of the wave length, the ambiguities are then to be fixed, in order to get the actual distance change. This makes it very difficult to use radar for epoch-wise measurements and deformations analysis.
Up to now, the area-wise measurement instruments are generally more expensive than the point-wise measurement instruments, so that they are installed usually temporally and measured epoch-wise instead of continuously, however, costs will be reduced in the future, similar to hardware of other instruments.
Although aforementioned disadvantages and challenges of the area-wise measurement methods, due to the high spatial sample of the object, the applying the area-wise measurement methods is the trend of the monitoring, some of their disadvantages can be came over by combing the point-wise measurement methods. Therefore, different types of the point-wise and area-wise measurement methods are combined in the project. Table 1 shows the characteristics of the terrestrial geodetic measurement methods used within the project regarding the monitoring application as an overview. Table 1 explains the characteristics of the different measurement methods in a condensed form. Additionally the opportunities for periodical or epoch-wise deformation analyses are summed up. As it will be shown in this article only GB-SAR is not usable for this task, since the geo-referencing is of much lower accuracy than the measurement accuracy of the method. Therefore, GB-SAR should be used for continuous measurements; in any case considering the current technical state.

Table 1: Characteristics of terrestrial geodetic measurement methods regarding monitoring

Measurement Method	Point- /area-wise measurement	Automation	Individual points needed	Accuracy (distance 100 m to 2 km)	Dimension of displacements	Epoch-wise deformation analysis possible
GNSS	point	yes	yes	mm to cm	3D	yes
Total Station	point	in principle yes	yes	mm to cm	3D	yes
TLS	area	yes	for epoch comparison	cm to dm	3D	yes
GB-SAR	area	yes	for epoch comparison	µm to mm	1D, line-of-sight direction	no

3. TEST SCENARIO LIANZIYA CLIFF

Situated on the west bank of the Yangzte River in the Hubei province, the National Geological Park of Three Gorges in Yangtze River Active Fault Garth of Fairy Mountain and Geo-hazard Garth of Xintan hosts one of the most disputed and complex natural structures of China, the rock cliff Lianziya. The opposite river side encompasses the more popular giant Xintan landslide and the Three Gorges Dam is situated at about 27 km from the cliff (fig.1). It is not only studied for its geological richness, but also for its potential of unleashing another natural catastrophe that would endanger the riverside inhabitant's life, waterborne transportation and the Three Gorges Dam. Lianziya Cliff is about 750 m high (from its base) and comprises a

geological structure mostly made out of limestone interbedded with thin shale located on the weak coal strata. On the outside, it looks like a precipice covered with cracks. The complete rock body has 13 large cracks and 58 small cracks, the largest of which is 5 meters wide, up to 170 meters long, 105 meters deep (Lu & Wang 2012). Several synthetic interventions were necessary to stabilize the cliff with special anchors (Guo et al., 1999). These are considered geotechnical engineering masterpieces, but despite this, the cliff is still prone to deformations.
Several historical events have pointed out that monitoring of landslides along the Yangtze can help at evacuating areas susceptible to flooding, stopping water traffic and taking all necessary measures before the slide occurs, thus preventing the loss of countless lives and economical losses (Guo et al., 1999). For this reason, scientists and engineers are working together in the attempt of preventing rock fall along the Yangzte River Basin on specific areas (cf. Yin et al. 2011) that show high potential of releasing large masses of rock/earth in the basin. Consequently causing waves up to 30 m that produce instant unimaginable damage and possibly completely blocking the river.
Specifically, in the case of the Lianziya Cliff, a research site has been established and among geological and geotechnical observation, geodetic measurements have been conducted for more than 20 years by the Research Institute of Rockfall & Landslide in Hubei Province, Three Gorges University. Within a DAAD (German Academic Exchange Service) and CSC (China Scholarship Council) cooperation project between the Institute of Engineering Geodesy from the University of Stuttgart (IIGS) and the School of Geodesy and Geomatics (SGG), Wuhan University, attention has been focused on epoch-based monitoring of the Lianziya Cliff. This was achieved on a yearly basis of local measurements with several geodetic methods commonly used in precise structural monitoring tasks. The overall scope is to identify movement tendencies and changes in hazardous areas of the Lianziya Cliff.

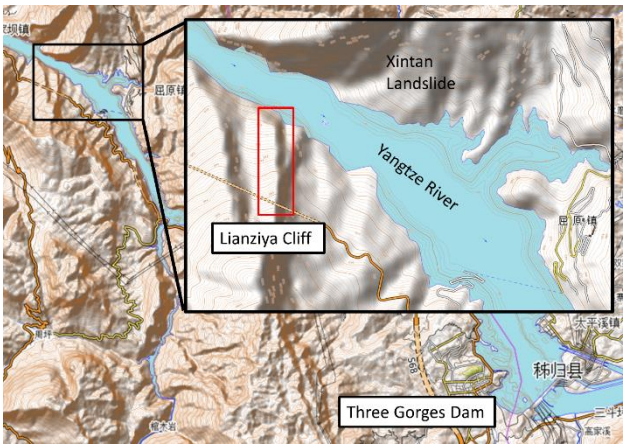

Figure 1 Location of the Lianziya Cliff on the Yangtze River (Source: opentopomap.org)

To overcome this challenge, several locations have been chosen according to the geodetic measurement method (see fig. 2). On the cliff's edge, several concrete pillars have been used for centring GNSS antennas and GB-SAR corner cube reflectors (CCR). The same pillars are used to mount the prisms used for the TS measurements. At the bases of the cliff, the topography permits two locations for measuring the exposed cliff side. These are used for TLS, TS, GB-

SAR and GNSS measurements. Location 1 is situated at ca. 750 m and location 2 at 125 m from the cliff (see fig. 2).
Not all methods have been implied in both epochs. Therefore, an overview is given with the ones used in 2018 and 2019 (tab. 2). Data measured with these sensors/methods are later on used for the geodetic data fusion within one epoch and between both epochs. Not all sensors contribute directly to the deformation analysis.

Table 2 Overview with the used sensors/methods in both epochs

Epoch	GNSS	TLS	TS	GB-SAR
March 2018	x	x		x
September 2019	x	x	x	x

Figure 2 Measurement locations and seismic areas of the Lianziya Cliff (Background source: Google Maps©)

This is the typical situation for monitoring cases. A client or an authority realizes the danger of a hazard e.g. a landslide or a rockslide as possible here, in Lianziya Cliff. Since a fast reaction is required, available methods are applied for a first analysis. During the progress of the monitoring, additional measurement methods may be used, since a detailed analysis of the geometry as well as of the deformation causes leads to new requirement. Supplementary, new technologies may be integrated. This situation is mirrored in table 2. In 2018 the monitoring was started with GNSS, TLS and GB-SAR. In 2019, total station measurements are added. Besides, GB-SAR measurements have two epochs have to be referenced. Other problems arise due to different reference points in both epochs. The term geo-referencing or even registration is an enormous challenge for this sort of inhomogeneous data. The identification of identical points in different data sets is of great importance. In the following, the authors will also focus on how and with which accuracy these issues were solved. Table 3 shows the information of the applied measurement methods in project as an overview.

Table 3 Overview of applied measurement methods in project

Type of Measurement Methods	Instrument Type	Accuracy	Spatial Resolution	Coordinate System
Point-wise				
GNSS	2018: Leica 1200 2019: Leica GM30	horizontal: 5mm+0.5ppm, vertical: 10 mm+0.5ppm (Leica 1200); horizontal: 8mm+1ppm, vertical: 15mm+1ppm (Leica GM30)	-	global (local for baselines)
Total Station	Leica TM30	0.15 mgon for horizontal angles 0.3 mgon for vertical angles 0.6 mm+1 ppm for distances	-	local
Area-wise				
TLS	Leica P50	120 - 270 m (location 2): 1.2 mm + 10 ppm 570 - 1000 m (location 1): 3 mm + 10 ppm for distance; 2.4 mgon for angles	22 cm (from location 1) 2.2 cm (from location 2)	local
GB-SAR	IBIS-L	Sub mm for the displacement in the LOS	Range resolution: 0.5 m Cross range resolution 4.4 mrad	local 2D

In the sections 4 and 5 the data acquisition methods, their processing and the data fusion are explained in detail, but before this, a brief description of how the link between data within one epoch is realised. Furthermore, the possibility of linking data between epochs is described.
Since the epoch from 2019 comprises all mentioned and used sensors (cf. tab. 2), it will be used as an example for linking data by means of point-wise and area-wise methods for one epoch. An exception to this is the GB-SAR data, which cannot be directly referenced in the same coordinate system. First, GNSS observations are made on two pillars in the active area and one ground point at location one (see Fig. 2). The same three points are measured by TS. Additionally, targets scanned by the TLS are also determined by TS observations and included in the network. This makes registration of the point clouds possible.
As regards the linkage between two epochs, several issues make the task challenging. The GNSS measurement are used to compute baselines (see section 4.1), but their absolute coordinates are not available. Therefore, only coordinate differences are used and integrated as baselines in the TS hybrid-network for 2019. There was no TS network in 2018. Therefore a direct connection between the TLS data of the two epochs is not given. This problem was solved by using areas considered stable in location 1, 2 and on the cliff's stable part. Thus with the help of an ICP algorithm, scans from 2018 were referenced in the system defined in 2019.

4. DATA ACQUISITION AND PROCESSING

4.1 GNSS

One GNSS-reference station (station R) was installed in location 1 (near the GB-SAR instrument) in a stable area, the antenna was mounted on one tripod. The reference station in 2018 and 2019 are close to each other but not the same. Two GNSS-rover stations (station M1 and M2) were installed near the cliff's edge (active area) on concrete pillars and both are in open sky location (compare figure 3 right). Therefore, two baselines (R-M1 and R-M2) could be measured (compare figure 3 left). They were measured in 2018 and 2019 in 2 hours with a

sample rate of 1 Hz. In 2018 Leica 1200 system (GPS only) and in 2019 Leica GM30 receiver (GPS+GLONASS+Beidou) are used. Two different GNSS receiver system are used, because the Leica 1200 system was not available in 2019. The given accuracy of these two receiver system are given Table 3, for a baseline length of ca. 0.7 km, the theoretical accuracy is ca. 5-9 mm in horizontal components and 10-16 mm in the height component. However, the accuracy of GNSS receiver system depends strongly on the obstructions in antenna vicinity.
Furthermore, besides the geodetic GNSS receiver system from Leica, low-cost GNSS receiver system from ublox (C94-M8P application board) were applied, the results have shown that the accuracy (standard deviation) are comparable (Zhang 2018, Zhang and Schwieger 2017, Zhang and Schwieger 2020). However, for the deformation analysis, only the results of the Leica receiver system are considered, because there is no antenna calibration file for applied low-cost GNSS antennas available, and one low-cost GPS antenna was calibrated and antenna phase center offset and variations are about several millimeters (Zhang and Schwieger 2017), the possible deformation between the two epochs is also millimeter to centimeter. The type calibration file of most geodetic GNSS antennas are available and they are used for the GNSS data processing.

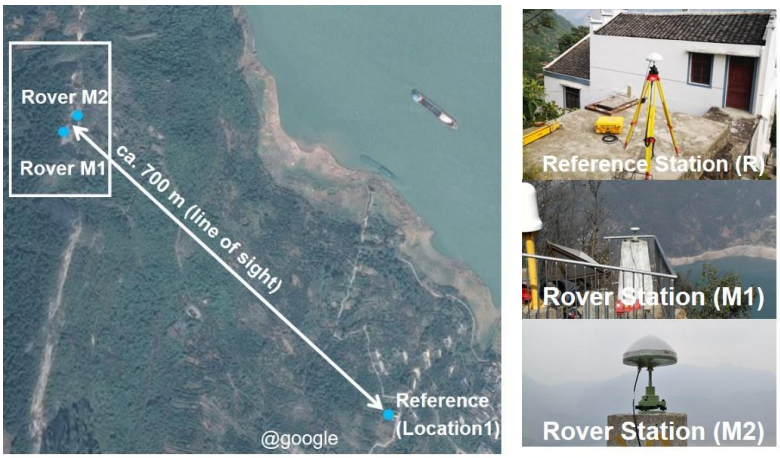

Figure 3: left: overview of the two baselines (Background source: Google Maps©) right: location of reference station and rover stations

Table 4 GNSS baselines of two epochs

Epoch	2018				2019			
Baseline	dE [m]	dN [m]	dh [m]	ds [m]	dE [m]	dN [m]	dh [m]	ds [m]
R-M1	-534.7696	423.3195	205.0149	712.1862	-534.7680	423.3363	205.0132	712.1940
R-M2	-546.9636	401.0483	211.3691	710.4124	-546.9654	401.0613	211.4005	710.4297

Table 5 Standard deviation of GNSS baseline of two epochs

Epoch	2018				2019			
Standard Deviation	sdE [mm]	sdN[mm]	sdh[mm]	sds [mm]	sE [mm]	sN[mm]	sh[mm]	sds [mm]
R-M1	3.9	3.7	12.2	13.4	4.5	3.0	13.5	14.6
R-M2	3.6	5.0	11.2	12.8	2.0	2.8	10.0	10.6

All GNSS data was processed in China using the GNSS baseline processing software wa2 (Wa2 2020). As aforementioned, the reference station in 2018 and 2019 are not the same. The reference stations in 2018 and 2019 are calculated separately by SGG using the nearby CORS stations of Chinese survey authorities. IIGS got only the coordinate difference of the reference in 2018 and 2019 in one coordinate system and used them for the deformation analysis later on. Table 4 and Table 5 show the baselines and their standard deviation (1σ) in east, north, height component and that of whole position for both epochs 2018 and 2019. The difference of baselines of two epochs are in mm to cm. The point-wise deformation analysis based on baselines will be given in section 6.1. Furthermore, compared with given standard deviation in their data sheets (see Table 3), the standard deviations in Table 5 are quite realistic and plausible. On the other side, these standard deviations obviously do not allow to detect the expected horizontal deformation of 4.2 mm / year for a temporal distance of one year (for vertical even worth). This means that for GNSS and a two-epoch comparison a longer temporal distance is required. If normal distribution is assumed, approximately 3 years are required for detection in the horizontal north-east direction.

4.2 Total Station

Total stations are among the most versatile geodetic instruments available. One may refer to modern TS instruments as multi-sensor systems. It is beyond this paper's scope to review TS features, therefore the reader is directed to Schwieger et al. (2020) for more technical details.
Due to their capability of measuring precise angles and distances, total stations are commonly used for creating engineering reference frames for construction or monitoring purposes (cf. Uren & Price, 2010). For this reason, a Leica TM30 and Leica GPR121 precision reflectors were used to create the connecting network for several measurement types at the Lianziya Cliff; in any case for 2019.
The network was designed to include observed points for other sensors into one TS network. There was no need to station and centre above a marked or signalized point. These observed points include three GNSS points, four TLS targets, two TLS station points, two CCR, six reflector marks on the GB-SAR base and the three TS station points. As far as possible, redundant measurements were made in two faces for each point from different TS station points. Figure 4 left shows the spatial distribution of the TS network points and gives information about which sensors where used at each location.

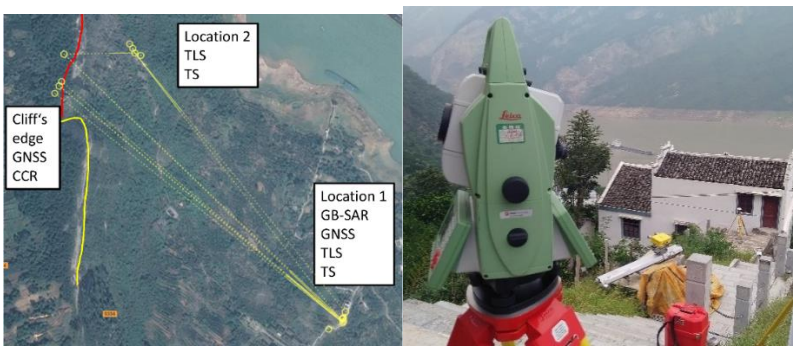

Figure 4 Left: TS network and sensors used at each location (Background source: Google Maps©), right: example of setup at location 1 with TS, GB-SAR and GNSS Receiver

All the data was gathered on the 09.09.2019 within slight varying atmospheric conditions. These were recorded with meteorology measurement stations placed in location 1, between the two locations and on the cliff's edge. Air temperature varied between 26°C and 28°C, relative humidity between 65% and 70% and air pressure between 972 hPa and 974 hPa. For these small variations and short timespan between measurements, it can be assumed that the distance measurement correction remains the same during the measurement in two locations.
In some cases, reciprocal measurements that implied exchanging the TS with the reflector directly through force centring on the tribrach where possible (e.g. TLS station point and TS station point), but in some cases this is impossible. In addition, some of the TLS targets where measured directly without a reflector. For the post-processing integration of GB-SAR data, an attempt of measuring the CCR was made. These were measured in a similar way with the TLS targets, without a reflector, even though the distances were of 717 m, respectively 746 m. These distances were at the limit of the maximum measurable range in the given conditions (Leica, 2020), but after successive attempts, the distances could be measured.
Finally, a least-squares network adjustment for the GNSS baselines and TS observations was conducted with the open source software JAG3D (Steinbeis Transfer Centre Applied Geodesy, 2020) and a local reference network was defined (fig. 5). To have an impression about the reached network quality, information is extracted from the main diagonal of the variance-covariance matrix (VCM) as quality indicators. For example, the square root of the trace of the VCM is 49 mm and 3D standard deviations for the observed points vary from 1.0 mm to 15.9 mm. In the horizontal plane, the error of position is in an interval from 1.5 mm to 19.3 mm. This is acceptable considering the reference network dimensions and atmospheric conditions. In addition, the ratio between the degrees of freedom (*f*) and observations in the network has a value of B=0.58 computed as follows: $B=f/n$ where $f=n-u+d$ and $n=86$, $u=39$ *and* $d=3$. This value is typical for terrestrial measurement adjustments. The before mentioned 3D standard deviation are in the same order of magnitude as the GNSS measurements and need temporal distances of 3 to 5 years to significantly detect expected deformations.

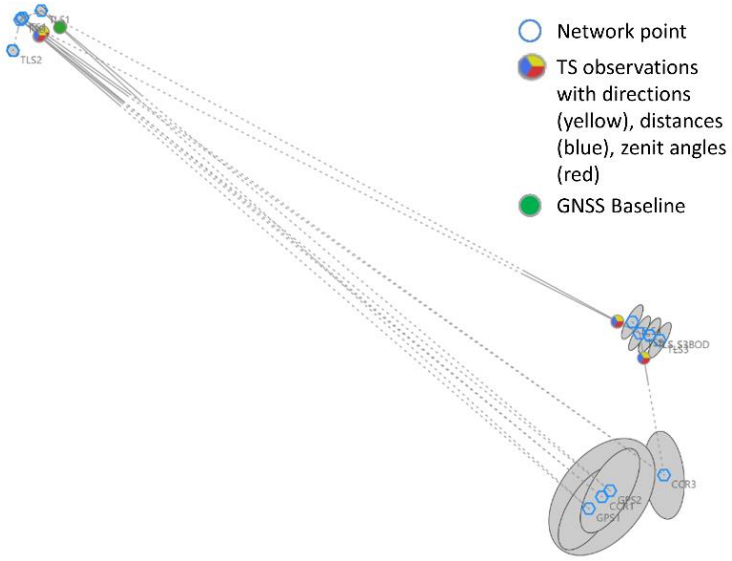

Figure 5: Network sketch with point distribution

4.3 TLS

Long range TLS has received much attention in rock cliff and land slide monitoring during the last decade (cf. Zangerl et al., 2008, Scaioni et al., 2013, Carrea et al., 2015, Huang et al., 2019, Dong et al., 2019). One main advantage is the level of detail in that can be reached for a large area. Particularly in the case of rock cliffs, it can be mentioned that the resulting point clouds represent the surface morphology very close to reality, mainly depending on the chosen TLS point spacing. Also referred to as point resolution, the point spacing depends on the angular increments of the laser scanner and the scanner position relative to the observed object. There are a multitude of interesting technical aspects related to TLS, but for more details the reader is advised to consult some of the available TLS publications (cf. Staiger, 2003, Wieser et al., 2019 Kuhlmann & Holst, 2018), just to name a few.

One issue that has not been solved yet is the deformation analysis method based on TLS point clouds (Wunderlich et al., 2016). The problems are mainly related to two aspects: firstly, the point cloud modeling method and secondly its stochastic model. In what regards the stochastic model of point clouds, advances have been made (cf. Kauker & Schwieger, 2017, Wujanz et al. 2017, Kerekes & Schwieger, 2020), but to the author's best knowledge there is still no commonly accepted method in the scientific community.
Nevertheless, TLS point clouds deliver valuable information about the detailed structure of the Lianziya Cliff, having no other equivalent in what regards level of detail when compared with the other four methods. The ranges that needed to be covered reach almost a kilometer, therefore impulse scanners are the only ones currently capable of scanning up to this distance. This was the main reason of choosing the Leica P50. According to its specification, it is considered a panorama scanner with a 45° rotating mirror and according to the used distance measurement system it is a time-of-flight scanner enhanced with Waveform Digitising (WDF) technology (Leica, 2020, Walsch, 2015). It disposes of two categories of measurement modes according to the desired range and uses two different wavelengths for the acquisition modes, both of them implying the laser class 1 scanning unit. With ranges up to 120 m and 270 m the 1550 nm invisible light is used. This is reaches range accuracies of 1.2 mm + 10 ppm over the entire range. In the other measurement modes that are used for distances up to 570 and 1000 m, the 658 nm visible light is used, offering accuracies of 3 mm + 10 ppm. Regardless of the distance measurement mode, the angular accuracy is 2.4 mgon for both horizontal and vertical angles (Leica, 2020).
Scans with the P50 were taken from both locations and in all cases, the scanner station point coincided with the TS station point. An important fact is that the tilt axis of the scanner is higher that the TS tilt axis when fixed on the same tribrach. This means that an offset between the physical axis intersection point of both instruments needs to be considered in the network adjustment. In case of the laser scanner, the tilt axis height is 250 mm, whereas the TS has a tilt axis height of 196 mm. As for the scanning parameters, at location 1 (approx. 700 m from the cliff) a scanning resolution of 3.1 mm@10 m was chosen. This means that the angular increments where 20 mgon leading to a point spacing on the cliff at an average distance of 715 m of ca. 22 cm. It is mentioned that the scan area included the active part of the Lianziya Cliff and a part of the stable area (see. figure 2). Additionally, areas considered stable near location 1 like fundaments, concrete pathway and neighbouring houses where scanned from the same station point. As regards the scans from location 2, the average distance from the TLS station

point to the cliff is ca. 135 m, therefore scanning in the measurement mode with distances up to 270 m, allowed a reduced scan time with a better resolution. In this case the resolution was set to 1.6 mm@10m, involving angular increments of 10 mgon and resulting in a point spacing on the cliff of about 2.2 mm. The resolution is improved by an average factor of 10 compared to location 1. This fact is essential for the registration that will be explained in section 5.1. To have an idea about the covered areas, the point clouds from both locations (depicted by long and short in the image) are presented in unique colours for each scan and epoch in figure 6.

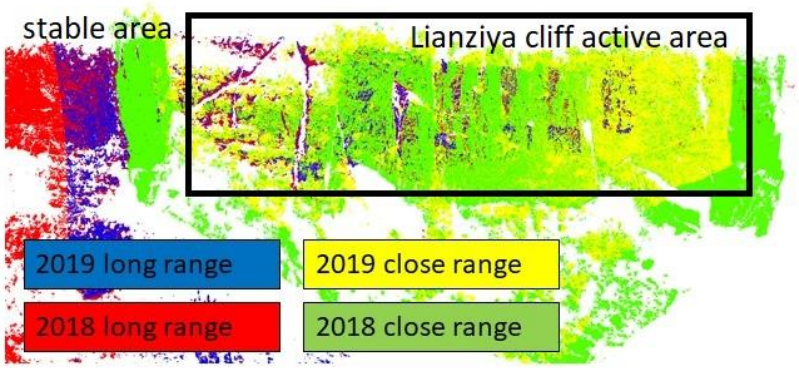

Figure 6 Point clouds from both locations coloured according to their position and epoch.

4.4 GB-SAR

The potential of GB-SAR for monitoring is been approved through a plenty of studies in the last two decades e. g. Leva et al. 2003; Herrera et al. 2009; Luzi et al. 2010; Rödelsperger 2011. GB-SAR is an active remote sensing technique and can be used therefore without direct contact to the monitored area and independent from day light. It uses the interferometric phase (e.g. the phase difference between successive acquisitions) for detection of distance change and thus the displacement in LOS-direction in each pixel of the 2D-image of the GB-SAR. The accuracy of this LOS-displacement is in sub-mm range. However, the maximum unambiguous detectable displacement is limited to the quarter of the wavelength. If displacement larger than this limit occurs between successive acquisitions, the term of ambiguity have to be determined and considered. This is challenging and requires further information about the real magnitude of the displacement. In order to avoid this, the GB-SAR is typically used for continuous monitoring of the area of interest for several days, so that the expected displacement between successive acquisitions is less than the unambiguous limit. Phase jumps (e.g. ambiguities) could be easily detected and fixed (temporal phase unwrapping). Nevertheless, epoch wise monitoring of artificial objects (e.g. dam) using GB-SAR is possible as well, thus the coherence remains strong enough on those objects (Tarchi et al. 1999; Wieser et al. 2020). A Further limitation of GB-SAR is that, the LOS-displacement does not represent neither the direction nor the magnitude of the real displacement. In order to get the real displacement based on GB-SAR measurement further information are required. Uncertainties in those information affect the accuracy of the monitoring results (see Hassan et al. 2018 & Hassan et al. 2019). Additionally the interpretation of GB-SAR measurement results is more complex compared to point wise measurements method or even TLS for example points at different heights and similar distances to the GB-SAR could contribute to the same pixel in the SAR-image.

Within this project, the GB-SAR instrument IBIS-L has been used. The instrument was fixed on a stable concrete fundament 700 m away from the active monitoring area. Due to the topography and obstacle within the sight, no better stations were available (near the monitoring area). The track of the instrument was leveled using an inclinometer. The elevation of the RADAR-Head was fixed to 10°. Further and as aforementioned two CCR were installed in the cliff near the GNSS-rover stations (see fig. 4). The same set up was used for both measuring epochs (2018 and 2019).
Within the measurement period of more than two days (e.g. 50 hours in 2018) a GB-SAR image was acquired approximately each six minutes (for both epochs). The maximum range was set to 1000 m. Due to unknown reason the range resolution (e.g. the pixel size) in range direction was unequal in both epochs (0.4999 m in 2019 and 0.5025 m in 2018). This difference of 2.5 mm/pixel leads to a shifting of several pixels in the active area at a range of almost 700 m.
In order to get possible best results just successive images without data gaps and acquired in good or rather relative constant atmospheric conditions were included in the processing. At the end 103 images from 2019 and 89 images from 2018 were selected. Those images were processed subsequently epoch wise. The steps of the epoch wise processing are described in a plenty of publication e.g. Rödelsperger 2011; Hassan et al. 2018. For this reason those steps will be mentioned just briefly in the following.
Firstly the phase and the amplitude were computed from the raw data in each pixel (and each image). In order to reduce the needed processing time just the data from the rock body and from the surrounding area (in the range from 600 m to 900 m and cross range from -25 gon to +25 gon) were included in the processing. The rest of the illuminated area is mainly covered by vegetation. For this reason, the data gathered there has bad quality. Within the included area the phase jumps in each pixel between successive acquisitions were detected and fixed. Subsequently the phase coherence was computed for each successive acquisition and the mean coherence (fig. 7) for each epoch was computed as well. This coherence shows a similar pattern in both epochs. The phase quality (e.g. coherence) at the rock body is clearly better (large values) than the quality at the surrounding areas.

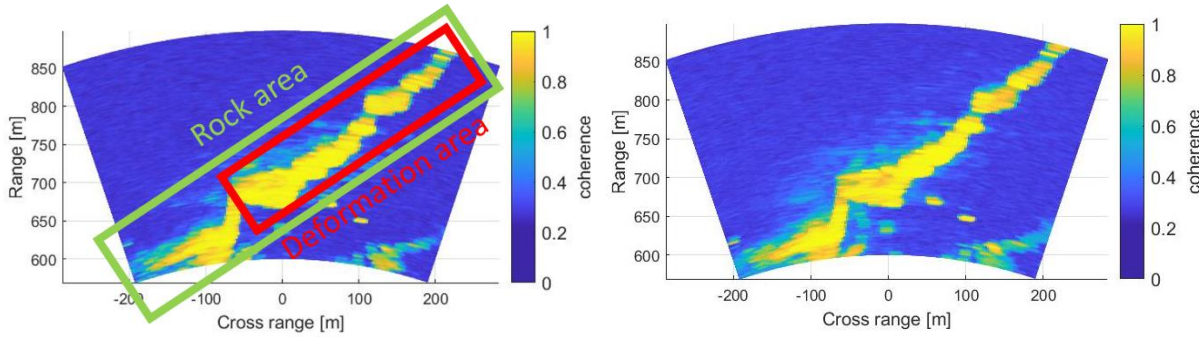

Figure 7: Coherence in 2019 (left) and in 2018 (right)

Based on the mean coherence five pixel with good coherence values were selected and used as ground control points (GCP) in order to determine the atmospheric phase and thus to do the atmospheric correction. After this correction, the LOS-displacement time series in each pixel are computed using the interferometric phase (e.g. the phase difference between successive

acquisitions within each epoch). Figure 8 shows those time series for four selected pixels within the deformation area in both epochs. The LOS-displacement time series show no significant deformation or clear trend. The deformation area could be considered as stable within the measurements period of each epoch.

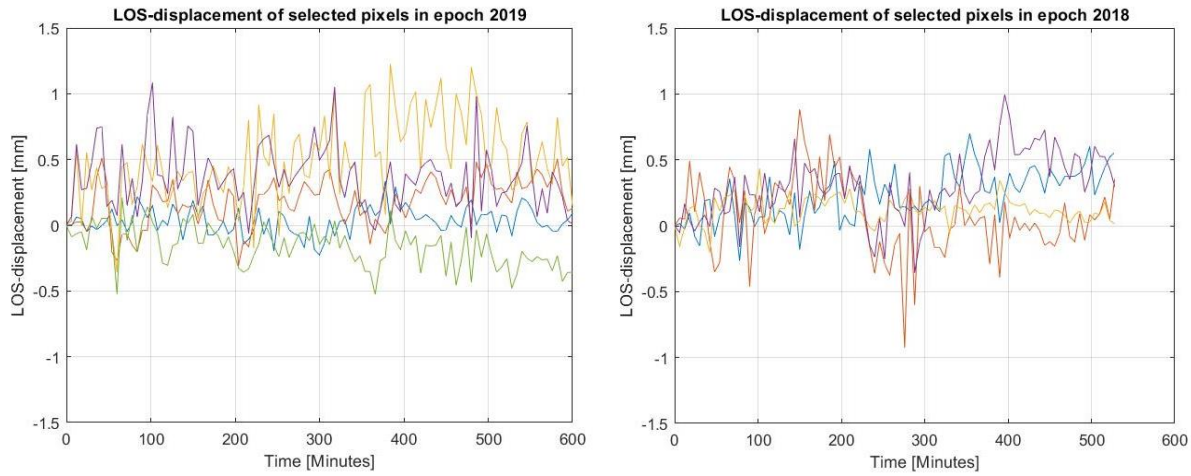

Figure 8: LOS-displacement time series for selected pixels in 2019 (left) and in 2018 (right)

Finally, the mean amplitude and the mean phase in each pixel were computed. Furthermore, the phase standard deviation was determined for all pixels besides those with bad quality outside the rock area. This standard deviation (fig. 9) will be used later in order to select the pixels, which will be included in the further processing (e.g. for the determination of LOS-displacement). As a threshold for this selection, a phase standard < 0.4 rad is required. This value is used in the literature in order to select persistent scatterers (PS) (Rödelsperger 2011; Ferreti et al. 2001).

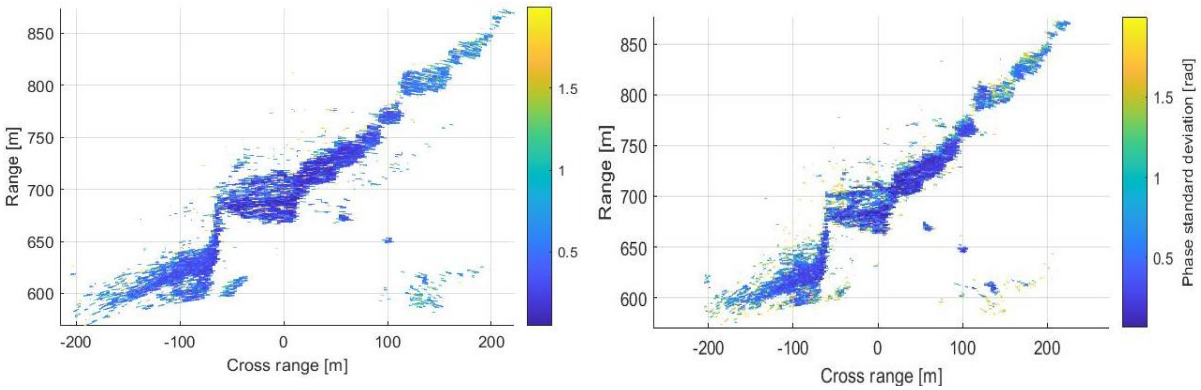

Figure 9: Phase standard deviation in 2019 (left) and in 2018 (right)

For GB-SAR as well as TLS (from 4.3) direct point accuracy values are not available due to the area-wise acquisition characteristic and the requirement for geo-referencing. Therefore, information will be given in section 5.

5. DATA FUSION

5.1 Registration of Point Clouds

By the term registration, multiple methods of aligning geodetic data to a certain coordinate system can be understood. To restrict the possible interpretations, it is mentioned that registration is used in this context as a mean of transforming data acquired in a local coordinate system (e.g. relative to the laser scanner) into another coordinate system defined with other geodetic instruments.

As known, TLS point clouds represent an object by means of Cartesian coordinates of millions of single points on that object. Usually several point clouds acquired from different station points are connected with one another with the help of direct or indirect registration. In the current case, indirect registration was used. The TLS point clouds were georeferenced in the TS reference system using the coordinates of the common points. The same points must be available in both measurement sets. In case of the TLS point clouds, Leica Tilt & Turn contrast targets were placed in the areas near the scanner at distances up to 50 m. The coordinates of the contrast targets middle point were extracted directly with the help of the software Leica Cyclone and then used for computing the transformations set necessary for registration. All contrast targets have coordinates in a local coordinate system defined by the laser scanner, which receives the origin coordinates. As mentioned before, the TLS station points are also included in the TS reference network. Having coordinates of common points in the two coordinate systems, the transformation parameters between the two sets can be computed. This is done with the help of a Helmert 6-parameter-transformation (cf. Niemeier, 2008). The three translations and three rotations are computed with the help of JAG3D and then applied on the complete point cloud with the help of a Matlab script. In this way, the point clouds acquired from both locations are in the same coordinate system within the 2019 epoch.

Since the same TS network is not available for the measurements in 2018, the point clouds acquired in that epoch need to be referenced in another way. This happened with the help of an ICP algorithm (cf. Besl & McKay, 1992, Somani et al. 1987) used by the open source software CloudCompare and applied on common features scanned in both epochs on stable areas. Firstly, a manual transformation is conducted with the help of identifiable common features like house corners, fundament corners or boulder edges to place the scans from 2018 in the same coordinates system with the ones in 2019. Afterwards, the fine alignment (ICP) is applied with six degrees of freedom. In other words, another 6-parameter-transformation set is determined based on the best fit found between common areas that are considered stable of the two point clouds. An example with overlapping areas is shown for in figure 10. The areas used for the fine alignment are highlighted.

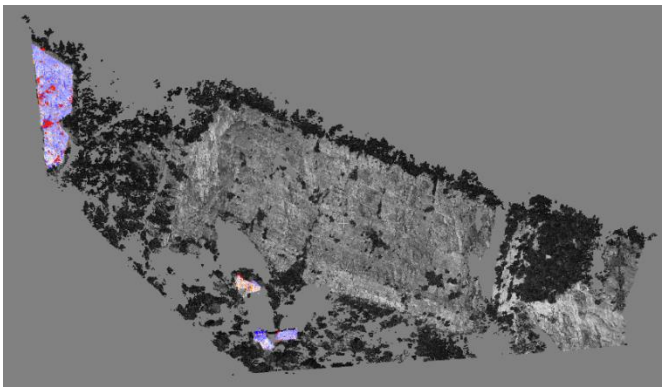

Figure 10 Lianziya Cliff with highlighted areas used for transforming the point clouds from 2018 into the 2019 coordinate system.

It is assumed that the areas remained the same within one year, but it is obvious that this cannot be completely true; therefore, the overlapping quote between two epochs is reduced from 100% iteratively until a plausible transformation is achieved. By this, the authors refer to a visible correspondence between features like edges that appear clear in both point clouds. Plausible results were obtained with an overlapping quote of 80%. To have a numeric indication about the transformation quality, the Root Mean Square (RMS) transformation error is given. Realistic epoch-overlapping registration is possible for point clouds that have the same point spacing, therefore the long range point clouds were aligned separately from the short range ones. This resulted in two different RMS values, for the long range scans (from location 1) the RMS is 9.3 cm and for the short range scans (location 2) the RMS is 7.3 cm. In the given situation, the results must be accepted since no better ways of registration for the two epochs are available. In normal TLS monitoring these values may be classified as too high, but it should be noted, that the transformations are made over natural feature (cliff areas) and even if stable as a whole, there is no straightforward method for evaluating if small changes occur at the surfaces of these stable areas. These values already make clear that the inhomogeneous TLS data needs a much higher temporal distance than 3 to 5 years as for the point-wise measurement methods.

5.2 Mapping of GB-SAR on TLS Data

The basic idea behind the data fusion concept proposed here is to exploit the advantages and avoid the disadvantages of each measurement technique. The advantage of GB-SAR is the high accuracy of the estimated LOS-Displacement. The disadvantages are, as aforementioned, the limitation of the estimated displacement to the LOS-direction and to the range of $\pm\frac{\lambda}{4}$. In order to overcome those disadvantages the results of TLS and/ or GNSS could be used to determine the direction and the magnitude (with less accuracy than the GB-SAR) of the real displacement. Using that information in addition to the transformation of the GB-SAR data into the same coordinate system as TLS and GNSS, the estimated LOS-Displacement can be projected on the direction of the real displacement and the ambiguity tem can be after that fixed using the estimated displacement magnitude from TLS or GNSS.

The most challenging step in this fusion procedure is the transformation step. In contrast to TLS, total station and GNSS, it is not enough to use the coordinate of the GB-SAR instrument

and the two CCR, measured by the TS for this transformation, but the direction of each LOS (e.g. each pixel) should be determined in the same coordinate system as the one used for TLS and GNSS.
For this transformation the distances S_i as well as the direction angles θ_i between the GB-SAR and each point within the TLS-point cloud were computed as following

$$S_i = \sqrt{\Delta X_i^2 + \Delta Y_i^2 + \Delta Z_i^2},$$

$$\theta_i = arctan\frac{\Delta X_i}{\Delta Y_i},$$

with $(\Delta X_i, \Delta Y_i, \Delta Z_i)$ being the coordinate differences between the GB-SAR and the point i from point cloud. The coordinates for the GB-SAR instrument are assumed to be the center of gravity of the six points measured on the GB-SAR- rail using total station.
Additionally the orientation O_0 of the GB-SAR in TS-coordinate system is needed. This orientation represents the direction angle of the mean SAR-LOS. This orientation can be determined through the difference between the direction angle of the line between the GB-SAR and one of the CCR in GB-SAR coordinate system and the direction angle of the same line in TS-coordinate system. Unfortunately, the CCRs could not be identified clearly in the GB-SAR data. Alternatively, the coordinate of the corner points of the GB-SAR rail are used for this purpose. This is not as accurate as using the CCR coordinates, due to the short length of the SAR Rail (2.3 m) compared to its range (up to 1000 m), but still the only available way to determine O_0. However, the orientation of the GB-SAR is assumed parallel to the short edges and perpendicular to the long edges of the rail. So the orientation could be determined 4 times and the average was used. This ordination O_0 is been subtracted subsequently from the angles θ_i in order to get the orientation O_i of each point within the point cloud in GB-SAR range by cross range coordinate system:

$$O_i = \theta_i - O_0$$

Using S_i and O_i each point in the point cloud be assigned to a specific pixel in SAR-image and get therefore the information extracted from GB-SAR data (e.g. range by cross range coordinates, coherence, phase standard deviation, LOS-displacement) as further attributes. From now on, the information extracted from GB-SAR and from TLS could be represented in the same coordinate system either in a 3D coordinate system (fig. 11) or in the 2D GB-SAR coordinate system (fig. 12)

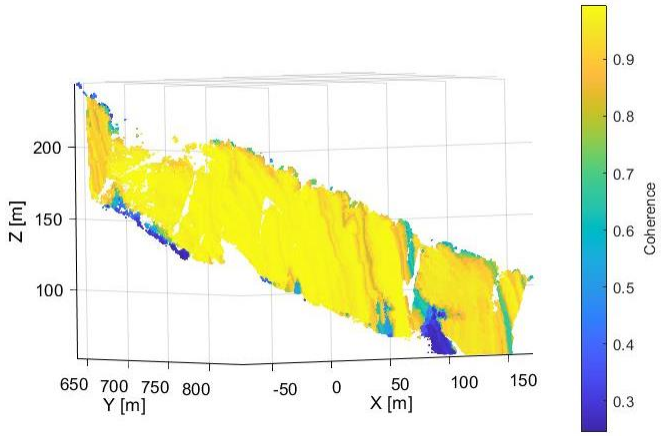

Figure 11: 3D Point cloud colored by the coherence values of the GB-SAR data from 2019

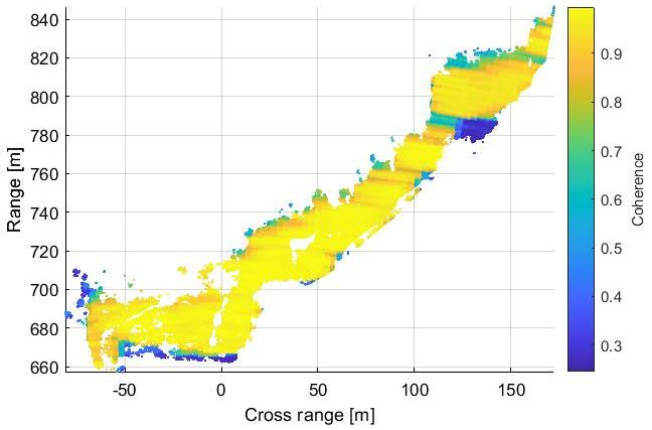

Figure 12: Point cloud mapped on the 2D GB-SAR coordinate system and colored by coherence of GB-SAR data from 2019

Figure 12 shows the same pattern for the coherence as the one shown in fig. 11 (down-left). This approves the validity of the transformation performed here.
Instead of using the point cloud for the transformation a DTM extracted from this point cloud can be used as well. The transformation will be more complex in this case.
The accuracy of the relative deformations in one epoch is below a mm (GB-SAR specific), but the accuracy for the deformation between two epochs relies on the accuracy of the mapping in LOS direction; here realized by TS and TLS measurements. So the accuracy is below the TLS accuracy of sections 4.2 and 4.3. The accuracy of the estimated real displacement is also very sensitive to the accuracy of the expected displacement direction, which can be either measured by other measurement techniques or determined based on geological or constructive models, and less sensitive to the accuracies of sensor and pixel positions (Hassan et al. 2019).

6. DEFORMATION ANALYSIS

6.1 Point-wise Deformation Analysis

For GNSS measurement, the change of the baselines (coordinate differences) can be calculated, as aforementioned in section 4.1. These differences are equivalent to the change of rover stations' position. Therefore, a point-wise deformation analysis can be conducted based on

GNSS baseline measurements. Table 6 shows the difference of baselines (based on Table 4) and the results of significant test.

Table 6 Deformation analysis of GNSS baseline of two epochs

	Baseline Differences (2018-2019)			Test values		
Baseline	ΔdE [mm]	ΔdN [mm]	Δdh [mm]	E	N	h
R-M1	-1.6	-16.7	1.7	0.15	1.58	0.07
R-M2	1.7	-13.0	-31.4	0.17	1.18	1.34

For the significant test, the standard deviation of the baselines in both epochs are considered (compare Table 5). Besides, the standard deviation of reference stations need also be considered, because their coordinates are calculated using the CORS stations. However, since there is no information about their accuracy available, the given accuracy in data sheets are taken (only the distance independent part). For example, standard deviation of baseline difference in east component is $s_{\Delta dE} = \sqrt{s_{dE\_2018}^2 + s_{dE\_2019}^2 + s_{ref\_E\_2018}^2 + s_{ref\_E\_2019}^2}$. The corresponding test value can be calculated by $t_{\Delta dE} = \left|\frac{\Delta dE}{s_{\Delta dE}}\right|$. The test values of the other coordinate components could be calculated in the same way and they are given in Table 6.
If all the test values are compared with the quantile of 1.96 (with an assumption of normal distribution and a probability of 95%), all of them are non-significant.

6.2 Area-wise Deformation Analysis TLS & GB-SAR

For the area-wise deformation analysis three methods are directly applied on the point clouds from two epochs. Holst et al. (2017) tested different methods implemented in Cloud Compare for detecting movements and deformations of natural and artificial features. The same three methods are like-wise used here. As regards the significance test, the same as in sec. 6.1 is performed here, with the mention that instead of the standard deviation of each single TLS measurement, a global value represented by the transformation RMS (cf. sec 5.1) is used. For location 1, the RMS is 9.3 cm and for location 2 the RMS is 7.3 cm. This means that for differences to be identified as statistically significant (normal distribution assumed and 5% significance, t-value=1.96), they need to be greater than 18.2 cm for the scans from location 1 and 14.3 cm for location 2.
In the first situation, further referred to as Cloud-2-Cloud (C2C) point clouds are compared directly with one another based on the nearest neighbour distance. In the scans from location 1, absolute distances between the two epochs (fig. 13 above) resemble only the different point spacing on the object (cliff). One may be tempted to think that deformations are present in the orange/red areas, but when analysing the situation on the scans from location 2 (fig. 13 down) it is clear that no deformation or tendency is evident. The majority of the points are classified in the blue/light green area with C2C distances from 0 to 22 mm distributed randomly all over the cliff area. Random scattered red/yellow/orange points are present in areas where vegetation is covering the cliff. This lead to the conclusion that with C2C, no displacement tendencies are identified in this case.

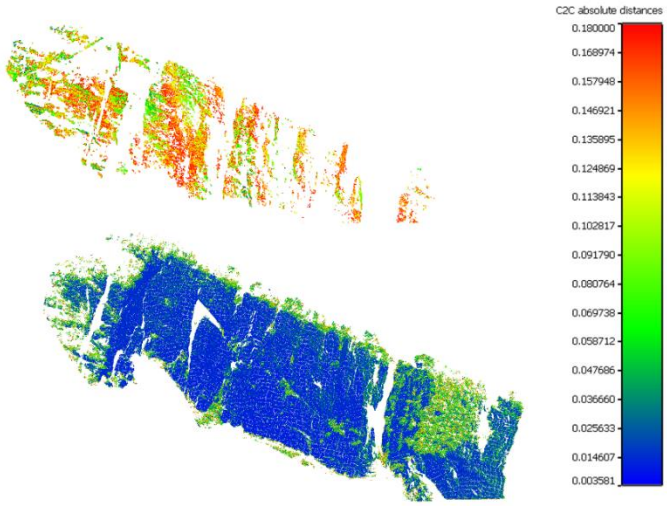

Figure 13 Lianziya Cliff C2C comparison. Long range scans above. Short range down.

The next method Cloud-to-Mesh (C2M) is more adequate in this case because firstly, a mesh is created for one point cloud and then points from the other are compared to this surface. It offers a more realistic image of the displacements if any are present because neighbouring points that may be outliers are not relevant as in C2C method. Note that the colour scale is adapted to represent positive and negative displacements (fig. 14). This shows regions that are either behind or in front of the created surface. Here it is clearer that no regions show distinguishable deformations.

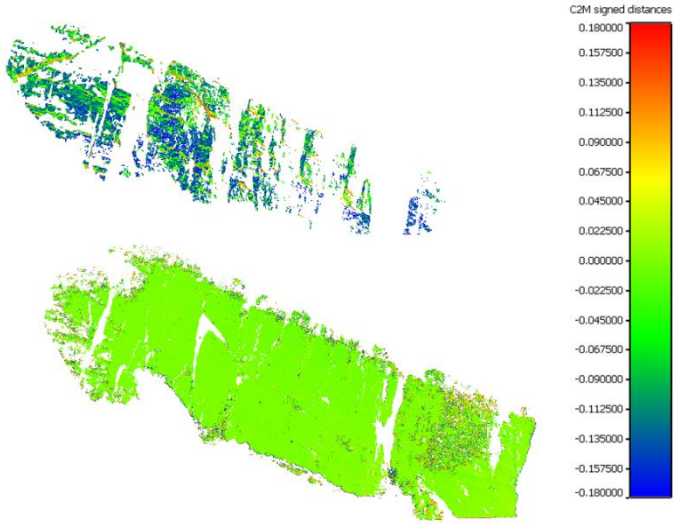

Figure 14 Lianziya Cliff C2M comparison. Long range scans above. Short range down.

The last method used for is called the multiscale model to model (M3C2) (fig. 15). An advantage when compared to the previous two is that surfaces are estimated for both point clouds and a sub-set of points that have computed normal are used for detecting differences between epochs. Moreover, 3D uncertainty information of the points is considered in the

analysis. It is beyond the scope of the current paper to present the method in detail, therefore the reader is advised to consult James et al. (2017) for a comprehensive view on the topic.
This method is the closest one to a classical geodetic deformation analysis in which the stochastic model characterizes the measurement uncertainty and considers it in decision making about possible deformations. In each case the 3D uncertainty for the points represents the transformation RMS (9.3 cm and 7.3 cm). An alternative would be to consider using either the Variance-Covariance Propagation Law (Niemeier, 2008), an intensity based stochastic model (Wujanz et al., 2017) or the elementary error model (Kerekes & Schwieger, 2020).
Finally, the subsampled points are placed on the same colour scale as in the C2M comparison. These do not reveal new findings, besides the areas that have already been identified in C2C and C2M method as being covered with vegetation. A possible improvement would be to denoise the point clouds according to Bitenc et al. (2019) and repeat the analysis.

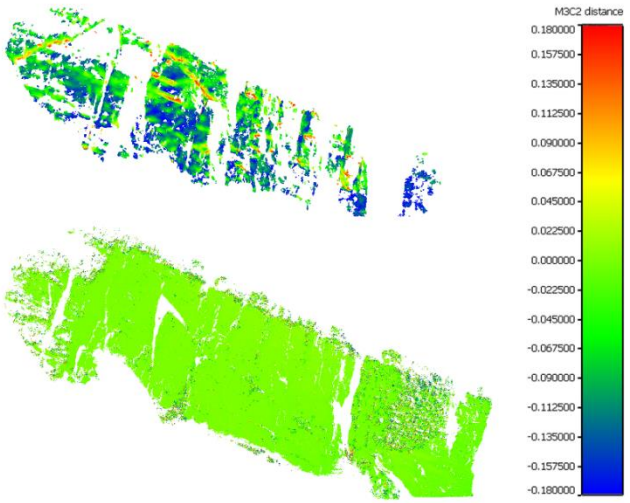

Figure 15 Lianziya Cliff M3C2 comparison. Long range scans above. Short range down.

These facts related to the area-wise deformation analysis are in concordance with the point-wise results, reconfirming that the cliff is considered stable for the analysed epochs. This does not mean that future deformations are not possible or to be expected, therefore monitoring of the Lianziya Cliff remains an issue that deserves further attention.

6.3 GB-SAR

Before applying the epoch comparison for GB-SAR data both epoch must be registered (e.g. transformed into the same GB-SAR coordinate system). For this purpose a 2 D cross correlation was implemented to the mean amplitude data of both epochs. The maximum correlation was achieved after shifting the 2019 data 8 pixels along the range direction. This shift fits to the difference in pixel size between both epochs (see 0) at a range of 750 m (the middle of the considered area). For this reason the data of 2019 was resampled to the same pixel size of the data from 2018. For this resampling the contribution of each original pixel to a resampled pixel was considered through a proper weighting function. The contribution of an original pixel to a resampled pixel was assumed to be the area from the resampled pixel, which is covered by the original pixel. The coherence between both epochs could be improved significantly through the

resampling (fig. 16). However, it is still clearly worse than the coherence within each epoch shown in fig. 11Figure . Even after the resampling just a small area in the middle of the active part and of the stable part of rock body have good (high) coherence values. The loss of coherence between both epochs could be caused by different states of the vegetation, which covers parts of the rock body, and different (average) atmospheric conditions between 2018 (March) and 2019 (September) measurement periods in addition to the different pixel sizes. However, the good coherence values belong to pixels where no or at least less vegetation cover exists (see fig. 17).

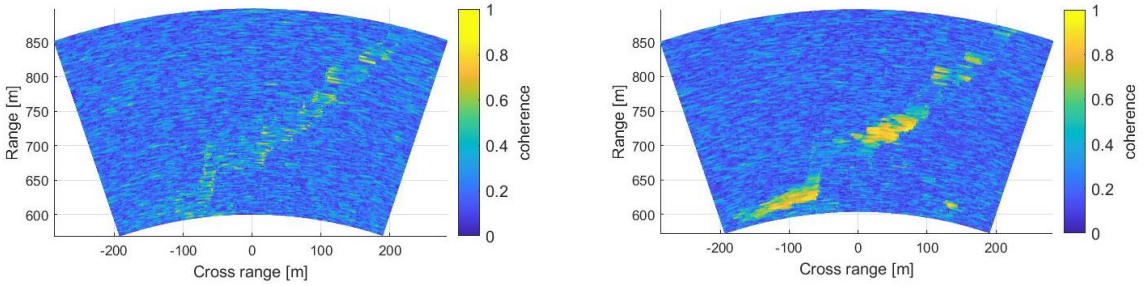

Figure 16: Coherence between 2018 and 2019 before the resampling (left) and after the resampling of 2019 data (right)

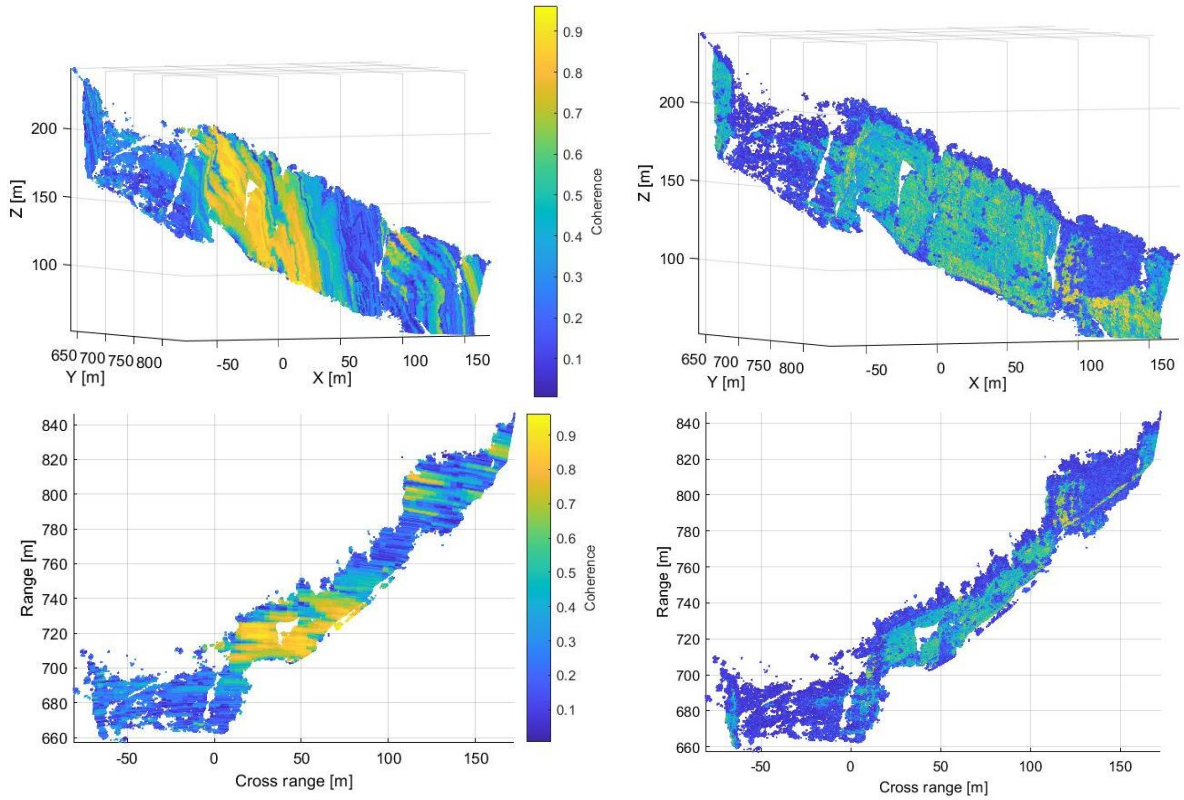

Figure 17: TLS point cloud colored by coherence between 2018 and 2019 (left) and by TLS intensity (right) in a 3D coordinate system (up) and mapped in the 2D GB-SAR coordinate system (down)

In addition to the aforementioned condition regarding the phase standard (see 0) in each epoch, the coherence between both epochs was considered in order to select the pixels used to extract the LOS-displacement. Just the pixels with a phase standard deviation (≤ 0.4 rad) in both

epochs and coherence > 0.8 were used for this purpose. Only 403 pixels full fill these conditions (for the comparison, just 3 pixels full fill these conditions without the resampling of 2019 data). For those pixels the interferometric phase (e.g. the phase difference between both epochs) was computed. Subsequently the LOS-displacement was determined from the interferometric phase. The estimated LOS-displacement after the resampling is shown in fig. 17. Due to the bad quality of the data and specially the gaps between selected pixels no spatial phase unwrapping was performed. Additionally the atmospheric effects between both epochs were not corrected.

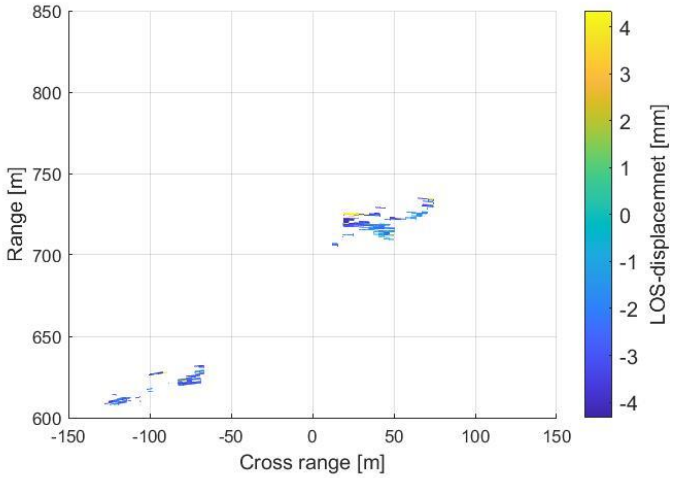

Figure 3: LOS-displacement between both epochs after resampling of 2019 data

The estimated LOS-displacement varies in the range of $\pm\frac{\lambda}{4} \approx \pm 4.3$ mm. This range represents the whole unambiguous measureable deformation range. The majority (90 %) of the selected pixels has a negative deformation values near the minimum measurable deformation ($-\frac{\lambda}{4}$). The rest of the selected pixels show a positive deformation near to the maximum measurable deformation value indicating a phase jump in those pixels. This issue could be addressed to the missing spatial phase unwrapping. Furthermore, the similar deformation pattern could be recognized in the active deformation area (in the middle of fig. 16Figure 3) as well as in the stable area (down left part of fig. 18) of the rock body. For this reason, the registered deformation could be related to the different atmospheric conditions between both epochs. Similar to the results of TLS and GNSS, the rock cliff could be considered as stable within the measurement period.

7. CONCLUSION AND OUTLOOK

This contribution shows the attempts to fuse inhomogeneous data of point-wise and area-wise measurement methods and analyze deformations. It deals with the well-known problems of fusing point-wise (GNSS and tachymeter) and area-wise methods (TLS and GB-SAR) as well as the detecting of deformation between two area-wise measured epochs in statistically correct way. These challenges are aggravated by the incompleteness of the data in the year 2018. Here no unique registration was realized, so that the coordinate systems of the TLS data and the GB-

SAR are not defined. By the way, for the GB-SAR this is method-inherent, for TLS this was a logistic error.
The TLS the challenge was solved by identifying stable areas in the scans of the two epochs and, in consequence, determine deformations for the remaining unstable areas only. The epoch-wise deformation analysis using GB-SAR data could not be solved. The mapping in LOS direction using TRS and TLS measurements was realized and it is a good way to enhance the interpretation of monitoring results of GB-SAR.
For the test scenario Lianziya Cliff no movements could be detected with the methods used, even if they are fused as in the case of tachymeter, GNSS and TLS as well as TLS and GB-SAR. The main reason for this fact is that the expected movements are well below the determined standard deviations. Thus, leading to non-significant statistical tests for the deformations. To have the opportunity to detect deformation, the second epoch should be measured more than three years after the first one. Even better is a time span of four to five years. The authors recommend to use GNSS and tachymeter measurements for geo-referencing and TLS measurements within distances of about 100 m to 200 m and to perform area-wise deformation analysis (preferably M3C2) with a high resolution. Additionally, a stochastic model that takes in consideration most of the error sources (e.g. a synthetic variance-covariance matrix should be integrated into the analysis. GB-SAR gives some additional interpretation support, but does not really help, because of the inaccurate geo-referencing of the two-epochs relative to each other. For future epochs, it may be omitted. If continuous monitoring is strived, GB-SAR is the adequate measurement tool providing significant deformations after a short time. If again the 4.2 mm horizontal deformation per year is expected, GB-SAR may deliver significant results after some months, if the meteorological corrections are take into account, because geo-referencing between epochs in not an issue anymore.
Obviously, the design of these monitoring measurements was not appropriate to detect the expected movements in a one-year period. Within this contribution, several short-comings of the design in the epochs 1 and 2 as well as occurred logistical faults are described. Nevertheless, hints are given to avoid these problems in the future and to provide a plan for future monitoring of the Lianziya Cliff after three, better five years.

ACHKNOWLEDGEMENT

The investigations published in this article are granted by the DAAD (German Academic Exchange Service) and CSC (China Scholarship Council) within PPP (Project Based Personnel Exchange Program) Project ID: 57446528. Therefore, the authors cordially thank the funding agencies and the colleagues from the Institute of Surveying Engineering, School of Geodesy and Geomatics, Wuhan University, Wuhan, P. R. CHINA, Jinjun Xu, Cheng Xing, Junbo Shi, Yaming Xu for their participation in data analysis and at the measurement campaigns.

REFERENCES

Besl, P.J., McKay, N.D. (1992) A method for registration of 3-D shapes. In: IEEE Transactions on pattern analysis and machine intelligence, 14(2), pp.239-256.

Bitenc, M., Kieffer, D.S. & Khoshelham, K. (2019) Range Versus Surface Denoising of Terrestrial Laser Scanning Data for Rock Discontinuity Roughness Estimation, In Rock Mechanics and Rock Engineering 52: 3103, Springer Vienna.

Carrea, D., Abellan, A., Derron, M.H., Jaboyedoff, M. (2015) Automatic Rockfalls Volume Estimation Based on Terrestrial Laser Scanning Data. In: Lollino G. et al. (eds) Engineering Geology for Society and Territory - Volume 2. Springer, Cham.

Dong, X., Xu, Q., Huang, R. et al. (2019) Reconstruction of Surficial Rock Blocks by Means of Rock Structure Modelling of 3D TLS Point Clouds: The 2013 Long‐Chang Rockfall, In: Rock Mechanics and Rock Engineering, Springer Vienna.

Engel, P., Foppe, K., Köster, U. (2020) Ingenieurgeodätisches Monitoring im Internet of Things – Entwicklung und Erprobung autonomer Sensorsysteme. In: Wunderlich, Thomas A. (eds), Ingenieurvermessung 20. ISBN 978-3-87907-672-7. Wichmann - VDE Verlag.

Engel, P., Foppe, K. (2016) Open Source Deformation Monitoring. A Multi-Plattform Approach for Automated Observation in Geodesy. In: Proceedings of GeoTerrace 2016, Lviv, Ukraine.

Guo, X.Z., Huang, X.B., Xu, K.X., Chen, W.M., Li, H.W., Tao, W.H. (1999) The control works of Lianziya dangerous rock mass and Huanglashi landslide in the Three Gorges of Yangtze river, Chin. J. Geol. Hazard. Control, Volume 10, Issue 4, pp. 15-34.

Hassan, A., Xu, J., Zhang, L., Liu, G., Schmitt, A., Xing, C., Xu, Y., Ouyang, C., Schwieger, V. (2018) Towards integration of GNSS and GB-SAR measurements: Exemplary monitoring of a rock fall at the Yangtze River in China, FIG kongress, Istanbul, 2018.

Hassan, A., Xu, J., Xing, C., Schwieger, V. (2019) A contribution to variance analysis of 3D-displacement extracted from GB-SAR measurements, Journal of Geodesy, Cartography and Cadastre - ISSN: 1454-1408.

Harmening, C., Neuner, H. (2017) Choosing the Optimal Number of B-spline Control Points (Part 2: Approximation of Surfaces and Applications). Journal of Applied Geodesy, Vol. 11 (2017), Issue 2; pp. 43 - 52.

Herrera, G.; Fernández-Merodo, J. A.; Mulas, J.; Pastor, M.; Luzi, G.; Monserrat, O. (2009) A landslide forecasting model using ground based SAR data: The Portalet case study, Engineering Geology, 105(3), 220-230.

Hesse, C., Neumann, I., Wodniok, J., Lippmann, G. (2016) Monitoring von Großbauwerken an der Schnittstelle zwischen Geodäsie, Bauingenieurwesen und Maschinenbau am Beispiel des Schiffshebewerkes Lüneburg. Zfv 5/2016 141 Jg. DOI 10.12902/zfv-0133-2016.

Heunecke, O., Glabsch, J., Schuhbäck, S. (2011) Landslide monitoring using low cost GNSS equipment - Experiences from two alpine testing sites. Journal of Civil Engineering and Architecture, Volume 5, Issue 8, S. 660-669.

Holst, C., Klingbeil, L., Esser, F., Kuhlmann, H. (2017) Using point cloud comparisons for revealing deformations of natural and artificial objects, Proceedings of INGEO 2017, 7th International Conference on Engineering Surveying, Portugal, Lisbon, ISBN 978-972-49-2300-0.

Huang, R., Jiang, L., Shen, X., Dong, Z., Zhou, Q., Yang, B., Wang, H. (2019) - An efficient method of monitoring slow-moving landslides with long-range terrestrial laser scanning: a case study of the Dashu landslide in the Three Gorges Reservoir Region, China, Landslides 16:839–855, Springer Berlin Heidelberg.

James, M. R., Robson, S., and Smith, M. W. (2017) 3‐D uncertainty‐based topographic change detection with structure‐from‐motion photogrammetry: precision maps for ground control and directly georeferenced surveys. Earth Surf. Process. Landforms, 42: 1769– 1788. doi: 10.1002/esp.4125.

Kauker, S., Schwieger, V. (2017) A synthetic covariance matrix for monitoring by terrestrial laser scanning. Journal of Applied Geodesy, Vol. 11, Issue 2, pp. 77-87.

Kerekes, G., Schwieger, V. (2020) Elementary Error Model Applied to Terrestrial Laser Scanning Measurements: Study Case Arch Dam Kops. *Mathematics* 2020, Vol. *8*, Issue 4.

Kuhlmann, H., Holst, C. (2018) Flächenhafte Abtastung mit Laserscanning - Messtechnik, flächenhafte Modellierung und aktuelle Entwicklungen im Bereich des terrestrischen Lasserscanning, In: Ingenieurgeodäsie - Handbuch der Geodäsie, ed. W. Schwarz, Springer-Verlag, ISBN 978-3-662-47187-6, Berlin, Germany

Leica Geosystems AG (2020) Leica TM30 Technical Specifications. URL: https://w3.leica-geosystems.com/, last accessed on 03.06.2020

Leica Geosystems AG (2020) Leica ScanStation P50 Technical Specifications. URL: https://w3.leica-geosystems.com/, last accessed on 03.06.2020

Leva, D., Nico, G., Tarchi, D., Fortuny-Guasch, J., Sieber, A. J. (2003) Temporal analysis of a landslide by means of a ground-based SAR interferometer, IEEE Transactions on Geoscience and Remote Sensing, 41(4), 745-752.

Lienhart W., Buchmayer F.S., Klug, F., Monsberger, C. (2019) Distributed Fiber Optic Sensing on a Large Tunnel Construction Site: Increased Safety, More Efficient Construction and Basis for Condition-Based Maintenance. In International Conference on Smart Infrastructure and Construction 2019 (ICSIC).

Lu, F. Wang, S. (2012) Application of the combined model in the deformation forecast of Lianziya hazardous rock mountain, *2012 IEEE International Conference on Computer Science and Automation Engineering (CSAE)*, Zhangjiajie, pp. 195-197, doi: 10.1109/CSAE.2012.6272578.

Luzi, G., Monserrat, O., Crosetto, M., Copons, R., Altimir, J. (2010) Ground-based SAR interferometry applied to landslide monitoring in mountainous areas, Mountain Risks conference: Bringing Science to Society, Firenze (IT), 24-26.

Niemeier, W. (2008) Ausgleichungsrechnung, 2nd ed.; Walter de Gruyter: Berlin, Germany.

Rödelsperger, S. (2011) Real-time processing of ground based synthetic aperture radar (GB-SAR) measurements, Dissertation Technische Universität Darmstadt, Fachbereich Bauingenieurwesen und Geodäsie.

Ryf A, Stengle R, Heiniger T (2017): Tunnelvermessung. In: Schwarz W. (eds): Ingenieurgeodäsie. Springer Reference Naturwissenschaften.

Scaioni, M., Roncella, R., Alba, M. I. (2013) Change detection and deformation analysis in point clouds: Application to rock face monitoring. Photogrammetric Engineering & Remote Sensing, Vol. 79, Issue 5, pp. 441-455.

Schill F, Eichhorn A (2017). Automatische Segmentierung von Profilscannermessungen am Beispiel von Brückenbauwerken. In: Ingenieurvermessung 17, Beiträge zum 18.Internationalen Ingenieurvermessungskurs Graz. Graz, Austria, Apr. 2017.

Schliefelbein N, Stemphuber W (2020) Geodätische Herausforderungen beim Brücken-Monitoring am Berliner Gleisdreieck. In: Wunderlich, Thomas A. (eds), Ingenieurvermessung 20. ISBN 978-3-87907-672-7. Wichmann - VDE Verlag.

Schwieger, V., Kerekes G., Lerke, O. (2020) Image-Based Target Detection and Tracking Using Image-Assisted Robotic Total Stations. In: Sergiyenko O., Flores-Fuentes W., Mercorelli P. (eds) Machine Vision and Navigation. Springer, Cham, https://doi.org/10.1007/978-3-030-22587-2_5.

Somani, A., Huang, T. S., Blostein, S. D. (1987). Least-square fitting of two 3-D point sets. IEEE Pattern Analysis and Machine Intelligence.

Staiger, R. (2003) Terrestrial Laser Scanning Technology - Systems and Applications. In: Proceedings of 2nd FIG Regional Conference, 2003, Marrakech, Morocco.

Steinbeis Transfer Centre Applied Geodesy (2020) Java Applied Geodesy 3D Software, URL: https://software.applied-geodesy.org/en/, accessed on 03.06.2020.

Tarchi, D., Rudolf, H., Luzi, G., Chiarantini, L., Coppo, P., Sieber, A. J. (1999) SAR interferometry for structural changes detection: A demonstration test on a dam, IEEE 1999 International Geoscience and Remote Sensing Symposium. IGARSS'99 (Cat. No. 99CH36293) (Vol. 3, pp. 1522-1524).

Tu, P.F., Wu, X.W. (2011) Study on Deformation and Failure Mechanism of Lianzi Cliff Dangerous Rock Body in Three Georges Reservoir Area, Subgrade Engineering, No.1/154, 38-40+44 (in Chinese language).

Uren, J., Price, B. (2010) Surveying for Engineers, 5th edition, Palgrave Macmillan, New York, USA.

Wa2 (2020) GNSS Baselines processing software. http://www.wasoft.de/wa2/, last access on 15.06.2020.

Walsh, G. (2015) Leica ScanStation P-Series – Details that matter, Whitepaper Leica Scan Station, retrieved from leica-geosystems.com, last accessed 08.10.2019.

Wang, S.Q. (1999) Monitoring and Forecast of Landslides in The Three Georges of Yangtze River, Geological publishing house (in Chinese language).

Wieser, A., Condamin, S., Barras, V., Schmid, L., Butt, J. (2020) Staumauerüberwachung–Vergleich dreier Technologien für epochenweise Deformationsmessungen, Beiträge zum 19. Internationalen Ingenieurvermessungskurs München, 2020, 437-449.

Wujanz, D., Burger, M., Mettenleiter, M., Neitzel, F. (2017) An intensity-based stochastic model for terrestrial laser scanners, ISPRS Journal of Photogrammetry and Remote Sensing, Vol. 125 (2017), p. 146-155.

Wunderlich, T., Niemeier, W., Wujanz, D., Holst, C., Neitzel, F., Kuhlmann, H. (2016) Areal Deformation Analysis from TLS Point Clouds – the Challenge, In: Allgemeine Vermessungsnachrichten 2016, Vol. 123, no. 11-12.

Wieser, A., Pfaffenholz, J-A., Neumann, I. (2019) Sensoren, Features und Physik - Zum aktuellen Stand der Entwicklung bei Laserscannern. In: Proceedings of TLS 2019 Seminar, DVW-Schriftreihe, Band 96/2019, Fulda, Germany, 2019.

Yi, W. (2006) Deformation Monitoring of T8-T12 Fracture Sections at Lianziya Cliff of Three Gorges, Disaster And Control Engineering. No.2/61, 28-32 (in Chinese language).

Yin, Y., Sun, P., Zhang, M., Li, B. (2011). Mechanism on apparent dip sliding of oblique inclined bedding rockslide at Jiweishan, Chongqing, China. Landslides. 8. 49-65. 10.1007/s10346-010-0237-5.

Zangerl, C., Prager, C., Brandner, R., Brückl, E., Eder, S., Fellin, W., Tentschert, E., Poscher, G., Schönlaub, H. (2008) Methodische Leitfaden zur Prozessorientierten Bearbeitung von Massenbewegungen, Geo.Alp, Institut für Geologie und Paläontologie, Universität Innsbruck Naturmuseum Südtirol.

Zhang, L., Schwieger, V. (2020): Reducing Multipath Effect of Low-Cost GNSS Receivers for Monitoring by Considering Temporal Correlations. Journal of Applied Geodesy, vol. 14, no. 2, 2020, pp. 167-175. https://doi.org/10.1515/jag-2019-0059.

Zhang L (2018) Low-Cost GNSS for geodetic applications. FIG Congress 2018, 06.-11.05.2018, Istanbul, Turkey.

Zhang L., Schwieger V. (2017) Investigation of a L1-optimized Choke Ring Ground Plane for a Low-Cost GPS Receiver-System. Journal of Applied Geodesy, Band 12, Heft 1, Seiten 55–64, ISSN (Online) 1862-9024, ISSN (Print) 1862-9016, DOI: https://doi.org/10.1515/jag-2017-0026.

Zhang L., Stange, M., Schwieger, V. (2012) Automatic Low-Cost GPS Monitoring System using WLAN Communication. In: Proceedings of FIG Working Week 2012, Rom, Italy.

CONTACTS

M.Sc. Aiham Hassan,
Dr.-Ing. Li Zhang,
M.Sc. Gabriel Kerekes,
Prof. Dr.-Ing. habil. Dr. h.c. Volker Schwieger

University of Stuttgart
Institute of Engineering Geodesy
Geschwister-Scholl-Str. 24 D
D-70174 Stuttgart
GERMANY
Tel. + 49/711-685-84049 | -84051 | -84040
Fax + 49/711-685-84044
Email: li.zhang@iigs.uni-stuttgart.de, gabriel.kerekes@iigs.uni-stuttgart.de,
volker.schwieger@iigs.uni-stuttgart.de
Web site: http://www.iigs.uni-stuttgart.de